NONLINEAR DYNAMICS AND ADAPTIVE CONTROL USING THE DYNAMIC INVERSION CONCEPT AND NEURAL NETWORKS FOR A GUIDANCE GYROSYSTEM (GG) WITH ONE GYROSCOPE AND TWO SUSPENSION GIMBALS (GAR) PART 1.OBTAINING THE NONLINEAR DYNAMIC MODEL

Constantin Adrian MIHAI[*], Romulus LUNGU[*,]**

[*]Politehnica University of Bucharest, Doctoral School of Aerospace Engineering, Bucharest, Romania
(adrianmihai10.07@gmail.com)
[**]Member IAA – International Academy Astronautics, Paris, France
(romulus_lungu@yahoo.com)

DOI: 10.19062/2247-3173.2025.26.18

Abstract: *This paper series presents a study on the nonlinear dynamics and adaptive control of the guidance (GG) with a fast astatic gyroscope in external gimbal suspension (GAR), using the concept of dynamic inversion and neural networks. In part 1, a new nonlinear dynamic model is derived for the GG placed on an aircraft (rocket), which expresses the GG dynamics relative to the absolute trihedron; generalized Euler equations are used for its dynamic elements (rotor-inner gimbal assembly and outer gimbal). The absolute angular velocities of the GG's dynamic elements have as components their angular velocities relative to the trihedron linked to the guidance line, and the perturbing angular velocities induced by the rocket's angular velocities around its axes. The obtained nonlinear equations are then expressed in equivalent forms, where the new variables are the angular rotation velocities of the guidance line (the target coordinator axis, i.e., the gyroscope's proper angular momentum axis). The angular rotation velocities of the guidance line are chosen as the output variables of the GG, with respect to which the relative degrees of the equations are equal to 2. The input variables of the nonlinear dynamic model are the command currents applied to the command coils of the motors located in the axes of the two gyroscopic gimbals, which create, by gyroscopic effect, correction angular velocities the orientation of the target coordinator axis (guidance line) in the direction of the target line. The obtained equations contain terms that are functions of the input and output variables, as well as terms that are functions of the transport angular velocities of the guidance line and perturbing terms (functions of the rocket's angular velocities).*

Keyords: *GG, GAR, guidance line, line of sigh.*

1. INTRODUCTION

Gyroscopic systems for orientation and stabilization represent an important category of gyrosystems, which are monoaxial or constructed on the principle of biaxial or triaxial force gyrostabilizers. These systems are used for orienting and stabilizing an axis (the target coordinator axis) along the guidance direction (an axis oriented towards a fixed point in space, called the target point). In the case of a platform with one, two, or three stabilization axes, the stabilized axis (guidance line) is the axis perpendicular to the plane of the stabilized platform, which can be terrestrial, maritime, aerial, or spatial [1-10].

The gyroscopes used are of the GAR type or speed gyroscopes, mounted on gimbals with mechanical suspension or magnetic suspension [11-18].

In most specialized works, the dynamic models used and the control laws are linear, the mathematical models being obtained by linearization around specific orientation and stabilization directions. Some works utilize nonlinear models without decoupling or with decoupling and independent control of dynamic elements (rotor, inner gimbal, outer gimbal) [9-11, 19-25].

In Part 1 of this paper series is presented the structure of the monoaxial GG with GAR, with the trihedrons and the associated angular magnitudes of the GG is presented (Section 2), new nonlinear forms of dynamic models are derived (Section 3), and conclusions are formulated in Section 4.

In Part 2 of this paper series is presented the design of the adaptive control architecture for the GG's stabilization and orientation using the Matlab/Simulink model, and the theoretical results are validated through numerical simulation.

2. GG STRUCTURE, TRIEDRAS AND ASSOCIATED ANGULAR MAGNITUDES

Such a guidance gyrosystem (GG), shown in Fig. 1, consists of the following subsystems: GAR; target coordinator (TC), located on the inner gimbal (IC); adaptive controller, consisting of two correction networks; gyroscopic gimbals rotation motors (CM1 and CM2). TC measures angular deviations α and β between its axis, that is, the line of sight (view) oz and the line of the target (guidance line) ox_T ,highlighted in Fig. 2.a.

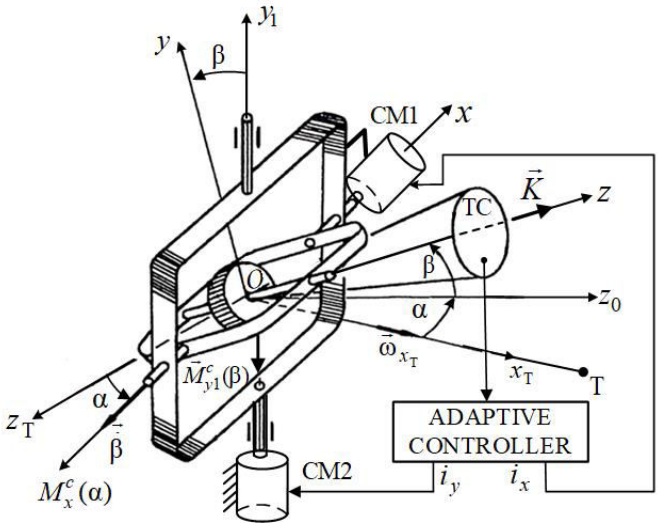

FIG.1 Guidance gyrosystem (GG) structure

The trihedron that refers to the base (the aircraft, A) is *OXYX*, the trihedron that refers to the outer gimbal (OG) is oxy_1z_0, the trihedron that refers to the inner gimbal (IG) is $oxyz$ (RESAL's trihedron) and the trihedron that refers to the target line (OT) is $ox_Ty_Tz_T$; the axis ox_T is oriented to the target (T), and oy_T and oz_T rotate around the axis ox_T with with angular velocity ω_{x_T}. The bearing of the target line is expressed by the angle λ (with the components λ_1 and λ_2 in the two planes), and the bearing of the line of sight is expressed by the angle δ (with the components δ_1 and δ_2 in the two planes).

The aircraft A rotates around its axes with angular velocities $\omega_X, \omega_Y, \omega_Z$. These generate angular velocity ω_{x_T} which, according to Fig.2.a, has the expression [12]

$$\omega_{x_T} = \frac{\omega_X \cos\lambda_1 - \omega_Z \sin\lambda_1}{\cos\lambda_2} \tag{1}$$

If ω_{x_T} would be null, the trihedron that refers to the target line would be $ox_T y'_T z'_T, \theta = 0$ and $\dot{\vec{\alpha}}$ oriented along the axis oy'_T oy'_1. But, because ω_{x_T} $\omega_X = \dot{\gamma} \neq 0$ it follows that the trihedron $ox_T y'_T z'_T$ rotates with angular velocity $\dot{\vec{\gamma}}$ (with angle γ) thus passing in $ox_T y_T z_T$.

Angular velocity of rotation of the target line (OT, ω_{x_T}) relative to the inertial frame of reference is ω_t (with the components ω_{t1} and ω_{t2}) and and the angular velocity of rotation of the target line relative to the trihedron connected to the base (A) is $\dot{\lambda}$ (with the components $\dot{\lambda}_1$ and $\dot{\lambda}_2$ in the two planes), $\vec{K}$ is the angular momentum of the gyroscope (the axis of the target coordinator TC).

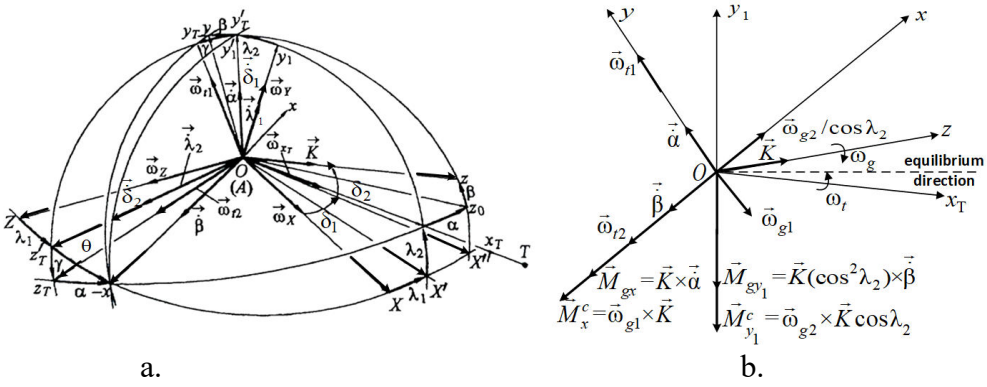

a. b.

FIG.2 Trihedral coordinate systems and related angular measurements GG

3. NONLINEAR FORMS OF GG DYNAMICS

To obtain the equations of the dynamics of GG with GAR, the generalized Euler equations of motion of the assembly (R+IG) – gyroscopic rotor + IG around the axis *ox* and of the outer gimbal (OG) around the axis oy_1 are used. These equations, for GAR located on a mobile base, are

$$\frac{\partial K_x^{R+IG}}{\partial t} + \Omega_y^{R+IG} K_z^{R+IG} - \Omega_z^{IG} K_y^{R+IG} = M_x^{R+IG}, M_x^{R+IG} = M_x \tag{2}$$

$$\frac{\partial K_x^{R+OG}}{\partial t} + \Omega_{z0}^{OG} K_x^{OG} - \Omega_x^{OG} K_{z0}^{OG} = M_{y1}^{OG} \tag{3}$$

the angular velocities of the assembly (R+IG), respectively of the outer gimbal OG, were indexed superiorly with (R+IG), IG or OG, suggesting that the respective dynamic element (R, IG,OG) does not rotate directly around the respective axis, mentioned by the (lower index).

From the relationship

$$M_{y1} = M_{y1}^{R+IG+OG} = M_{y1}^{OG} + M_{y1}^{R+IG} = M_{y1}^{OG} + M_y^{R+IG}\cos\beta + M_z^{R+IG}\sin\beta \tag{4}$$

is expressed M_{y1}^{OG}

$$M_{y1}^{OG} = M_{y1} - M_y^{R+IG}\cos\beta - M_z^{R+IG}\sin\beta \tag{5}$$

$$M_y^{R+IG} = \frac{\partial K_y^{R+IG}}{\partial t} + \Omega_z^{IG}K_x^{R+IG} - \Omega_x^{R+IG}K_z^{R+IG} \tag{6}$$

$$M_z^{R+IG} = \frac{\partial K_z^{R+IG}}{\partial t} + \Omega_x^{R+IG}K_y^{R+IG} - \Omega_y^{R+IG}K_x^{R+IG} \tag{7}$$

$$\Omega_x^{R+IG} = \Omega_x^R = \Omega_x^{IG}, \Omega_y^{R+IG} = \Omega_x^R = \Omega_x^{IG} \tag{8}$$

$$\begin{aligned}
&K_x^{R+IG} = K_x^R + K_y^{IG}, K_y^{R+IG} = K_y^R + K_y^{IG}, K_z^{R+IG} = K_z^{R+IG} = K_z^R + K_z^{IG}\\
&K_x^R = A\Omega_x^R, K_y^R = B\Omega_y^R, K_z^R = C\Omega_z^R\\
&K_x^{IG} = A_1\Omega_x^{IG}, K_y^{IG} = B_1\Omega_y^{IG}, K_z^{IG} = C_1\Omega_z^{IG}\\
&K_x^{OG} = B_2\Omega_x^{OG}, K_{y1}^{OG} = A_2\Omega_{y1}^{OG}, K_{z0}^{OG} = C_2\Omega_{z0}^{OG}
\end{aligned} \tag{9}$$

$A,B = A,C$ are the moments of inertia of R about to the axes of the trihedron $oxyz$, A_1, B_1, C_1 - the moments of inertia of IG about the axes of the trihedron $oxyz$ and A_2, B_2, C_2 - the moments of inertia of OG about the axes of the trihedron oxy_1z_0.

The absolute angular velocities, with the following expressions, are expressed as sums between the angular velocities of the dynamic elements (R, IG, OG) relative to the trihedron connected to the target line $ox_Ty_Tz_T$, angular transport velocities of the target line ω_{t1} and ω_{t2}, ω_{xT}, with respect to the inertial trihedron and angular velocities $\omega_x, \omega_y, \omega_z$ induced by angular velocities $\omega_X, \omega_Y, \omega_Z$ of the base (A); according to Fig.2.a,

$$\begin{aligned}
&\Omega_x^R = -(\beta + \omega_{t2}\cos\alpha + \omega_{x_T}\sin\alpha) + \omega_x \;\square\; -(\dot\beta + \omega_{t2} + \omega_{x_T}\alpha) + \omega_x\\
&\Omega_y^R = \dot\alpha\cos\beta + \omega_{t1} - \omega_{x_T}\cos\alpha\sin\beta + \omega_y \;\square\; \dot\alpha + \omega_{t1} + \omega_{x_T}\beta + \omega_y\\
&\Omega_z^R = \dot\varphi + \Omega_z^{IG} = \dot\varphi + \dot\alpha\sin\beta + \omega_{x_T}\cos\alpha\cos\beta + \omega_z \;\square\; \dot\varphi + \dot\alpha\beta + \omega_{x_T} + \omega_z\\
&\Omega_x^{IG} = \Omega_x^R, \Omega_y^{IG} = \Omega_y^R, \Omega_x^{OG} = \omega_x, \Omega_{y_1}^{OG} = \dot\alpha + \omega_y\cos\beta \;\square\; \dot\alpha + \omega_y, \Omega_{z0}^{OG} = \omega_z\cos\beta \;\square\; \omega_z
\end{aligned} \tag{10}$$

With $\dot\varphi$ the angular velocity of rotation of the gyroscopic rotor R was denoted. The angular velocities $\omega_x, \omega_y, \omega_z$ have the following expressions

$$\begin{aligned}
&\omega_x = -\omega_X\sin(\lambda_1 + \theta) - \omega_z\cos(\lambda_1 + \theta) \;\square\; \omega_X\sin\lambda_1 - \omega_Z\cos\lambda_1\\
&\omega_y = -\omega_X\cos\delta_1\sin\delta_2 + \omega_Y\cos(\lambda_2 + \beta) + \omega_Z\sin\delta_1\sin\delta_2 \;\square\; -\omega_X\cos\lambda_1\sin\lambda_2 +\\
&\quad + \omega_Y\cos\lambda_2 + \omega_Z\sin\delta_1\sin\delta_2 = -\omega_{x_T}\sin\lambda_2\cos\lambda_2 + \omega_Y\cos\lambda_2\\
&\omega_z = \omega_X\cos\delta_1\cos\delta_2 - \omega_Z\sin\delta_1\cos\delta_2 \;\square\; \omega_X\cos\lambda_1\cos\lambda_2 - \omega_Z\sin\delta_1\cos\delta_2 = -\omega_{x_T}\cos\lambda_2
\end{aligned} \tag{11}$$

The moments acting about the axes ox and oy_1 are expressed as sums of the disruptive moments $(M_x^e$ and $M_{y1}^e)$ with dynamic damping moments $(M_x^v$ and $M_{y1}^v)$ and with correction moments $(M_x^c$ and $M_{y1}^c)$

$$M_x = M_x^e + M_x^v + M_x^c, M_{y1} = M_{y1}^e + M_{y1}^v + M_{y1}^c \tag{12}$$

Given that the external disruptive moments are produced by the angular velocities of the base $\omega_X, \omega_Y, \omega_Z$, will be omitted from now on M_x^e and M_{y1}^e, their role being taken by the disruptive moments generated by these angular velocities. The dynamic damping moments are expressed as

$$M_x^v = F_x\dot{\delta}_2 \cos\theta \square F_x\dot{\lambda}_2, M_{y1}^v = -F_y\dot{\delta}_1 \square F_y\dot{\lambda}_1 \tag{13}$$

with $\dot{\lambda}_1$ and $\dot{\lambda}_2$ by forms

$$\begin{aligned}\dot{\lambda}_1 &= \frac{\dot{\alpha}+\omega_{t1}}{\cos\lambda_2} - \frac{\omega_{x_T}\beta}{\cos\lambda_2} + \omega_X\cos\lambda_1 - \omega_Z\sin\lambda_1 - \omega_Y \\ \dot{\lambda}_2 &= \dot{\beta} + \omega_{x_T}\alpha - \omega_X\sin\lambda_1 - \omega_Z\cos\lambda_1\end{aligned} \tag{14}$$

Equations (3) and (1) for ox and oy_1, with (5) ÷ (12), become

$$\begin{aligned}&B_0\ddot{\alpha} + [F_y - (A+B_1)\omega_{t2}]\dot{\alpha} + \omega_{x_T}(\omega_{t1} + \omega_{x_T}\sin^2\lambda_2)\alpha + [K\cos^2\lambda_2 + (B_1 - A_1)\omega_{x_T}]\dot{\beta} + \\ &+(A+B_1)(\omega_{t1} + \omega_{x_T}\omega_{t2}\dot{\omega}_{x_T})\beta + (A+B_1)\omega_{x_T}^2\alpha\beta - (A+B_1)\omega_{x_T}\dot{\alpha}\alpha - A_0\omega_{t2}\alpha\beta\cdot\omega_{x_T}\beta\dot{\beta} - \\ &-A_0\beta\dot{\alpha}\dot{\beta}(A+B_1)\alpha\dot{\beta} + K\omega_{x_T}\alpha\beta\dot{\alpha} + +C\beta\dot{\alpha}\dot{\beta} - M_{y1}^c(\beta) = -K\omega_{t2}\cos^2\lambda_2 - B_0\dot{\omega}_{t1} + \\ &+F_y(\omega_Y\cos\lambda_2 - \frac{1}{2}\omega_{x_T}\sin^2\lambda_2 - \omega_{t1}) - (A_2+C_1)\frac{1}{2}\dot{\omega}_{x_T}\sin^2\lambda_2 - -\omega_{t1}\omega_Y\tan\lambda_2 - \\ &-\omega_{t1}\omega_X\cdot\sin\lambda_2\tan\lambda_2 + \omega_{x_T}\omega_{t2}\cos^2\lambda_2 + (A_2+B_2-C_2)[\omega_X\omega_Y\cos^2 2\lambda_1 + \frac{1}{2}(\omega_X^2 - \omega_Y^2)\sin 2\lambda_1] \\ &A_0\ddot{\beta} + F_x\dot{\beta} + K\omega_{x_T}\beta + (-K + D_0\omega_{x_T})\dot{\alpha} + (A_0\dot{\omega}_{x_T} + F_x\omega_{x_T})\alpha - (C+C_1)(\omega_{t1}\omega_Y)\dot{\alpha}\beta + \\ &+E_0\dot{\alpha}^2\beta + E_0\omega_{x_T}\dot{\alpha}\beta^2 + M_x^c(\alpha) = K\omega_{t1} + A_0\dot{\omega}_{t2} + F_x(\omega_X\sin\lambda_1 + \omega_Z\cos\lambda_1 - \dot{\omega}_{t2})\end{aligned} \tag{15}$$

From the stability conditions, the correction moments $(M_x^c$ and $M_{y1}^c)$ have the same signs as the correction moments:

$M_{gx} = -K\dot{\alpha}$ and $M_{gy_1} = M_{gy}\cos\beta\cos\lambda_2 \square M_{gy}\cos\lambda_2 = -K(\cos^2\lambda_2)\dot{\beta}$;

The correction moments are chosen by next forms

$$\begin{aligned}M_x^c &= -k_1\alpha = -r_1K\alpha = K\omega_{g1}, M_{y1}^c = M_y^c\cos\beta\cos\lambda_2 \square M_y^c\cos\lambda_2 = \\ &= -k_2\beta\cos\lambda_2 = -r2(K\cos\lambda_2)\beta = K(\cos\lambda_2)\omega_{g2}\end{aligned} \tag{16}$$

with the notations

$$\begin{aligned}&\omega_{g1} = -r_1\alpha, \omega_{g2} = -r_2\beta, r_1 = k_1/K, r_2 = k_2/K, F_x/K = f_x, F_y/K = f_y, \\ &B_0/K = b_0, A_0/K = a_0, A/K = a_3, A_1/K = a_1, A_2/K = a_2, B_1/K = b_1, \\ &B_2/K = b_2, C/K = c, C_1/K = c_1, C_2/K = c_2, D_0/K = d_0 = A_0 - (C-C_1)/K, \\ &E_0/K = e_0 = [(C+C_1) - (B+B_1)]/K,\end{aligned} \tag{17}$$

the ecuations (15) becomes

$$
\begin{aligned}
&b_0\ddot{\omega}_{g1}+[f_y-(a_3+b_1)\omega_{t2}]\dot{\omega}_{g1}+(\omega_{x_T}\omega_{t1}+\omega_{x_T}^2\sin^2\lambda_2)\omega_{g1}+\frac{r_1}{r_2}[\cos^2\lambda_2+\\
&+(b_1-a_1)\omega_{x_T}]\dot{\omega}_{g2}+r_1(a_3+b_1)(\omega_{t1}+\omega_{x_T}\omega_{t1}+\dot{\omega}_{x_T})\omega_{g2}-\frac{a_3+b_1}{r_2}\omega_{x_T}^2\omega_{g1}\omega_{g2}-\\
&-\frac{a_3+b_1}{r_1}\omega_{x_T}\omega_{g1}\dot{\omega}_{g1}+\frac{a_0}{r_2}\omega_{t2}\dot{\omega}_{g1}\dot{\omega}_{g2}+\frac{r_1}{r_2^2}(a_3+b_1)\cdot\omega_{x_T}\omega_{g2}\dot{\omega}_{g2}-\frac{a_0}{r_2^2}\dot{\omega}_{g1}\omega_{g2}\dot{\omega}_{g2}+\\
&+\frac{a_3+b_1}{r_2}\omega_{g1}\dot{\omega}_{g2}+\frac{\omega_{x_T}}{r_1r_2}\omega_{g1}\dot{\omega}_{g2}\omega_{g2}+\frac{c}{r_2^2}\dot{\omega}_{g1}\omega_{g2}\dot{\omega}_{g2}+r_1(\cos\lambda_2)\omega_{g2}=r_1(\cos^2\lambda_2)\omega_{t2}+N_y(t)\\
&a_0\ddot{\omega}_{g2}+f_x\dot{\omega}_{g2}+\omega_{x_T}\omega_{g2}\frac{r_2}{r_1}(1+d_0\omega_{x_T})\dot{\omega}_{g1}+\frac{r_2}{r_1}(a_0\dot{\omega}_{x_T}+f_x\omega_{x_T})\omega_{g1}-\frac{c+c_1}{r1}(\omega_{t1}+\omega_Y)\dot{\omega}_{g1}\omega_{g2}+\\
&+\frac{e_0}{r_1^2}\dot{\omega}_{g1}^2\omega_{g2}+\frac{e_0}{r_1r_2}\omega_{x_T}\dot{\omega}_{g1}\omega_{g2}\dot{\omega}_{g2}-r_2\omega_{g1}=-r_2\omega_{t1}+N_x(t)
\end{aligned}
\tag{18}
$$

Where $N_x(t)$ and $N_y(t)$ are perturbation terms that do not contain the angular velocities ω_{g1},ω_{g2} and accelerations $\dot{\omega}_{g1},\dot{\omega}_{g2}$, that is, they contain only external disruptive terms;

$$
\begin{aligned}
&N_x(t)=-r_2a_0\dot{\omega}_{t2}-r_2f_x(\omega_Y\sin\lambda_1+\omega_Z\sin\lambda_1-\omega_{t2}\\
&N_y(t)=-r_1b_0\dot{\omega}_{t1}-r_1f_y(\omega_Y-\frac{1}{2}\omega_{x_T}\sin2\lambda_2-\omega_{t1})-r_1(a_2++c_1)\cdot\\
&\cdot(\frac{1}{2}\dot{\omega}_{x_T}\sin2\lambda_2-\omega_{t1}\omega_Y\cdot\tan\lambda_2\omega_{t1}\omega_X\sin\lambda_2\tan\lambda_2+\omega_{x_T}\omega_{t2}\cos^2\lambda_2)-\\
&-r_1(a_2+b_2-c_2)\cdot[\omega_X\omega_Y\cos2\lambda_1+\frac{1}{2}(\omega_X^2-\omega_Y^2)\sin2\lambda_1]\cos\lambda_2
\end{aligned}
\tag{19}
$$

In the absence of disturbances $(N_x(t)=N_y(t)=\omega_{x_T}=\dot{\omega}_{x_T}=0)$, that is, **in orientation mode**, with $\omega_{t1}=\text{const.}$ and $\omega_{t2}=\text{const.}$, at equilibrium $\omega_{g1}=\text{const.}=\omega_{t1}$ and $\omega_{g2}=\text{const.}=\omega_{t2}\cos\lambda_2$ (for $M_x^c/K=\omega_{g1}$ and $M_y^c/K=\omega_{g2}$); the sighting line tends to follow the target line, which, in turn, overlaps the equilibrium direction (the straight line with the dashed line in Fig.2.7.b resulting from the rotation of the axis ox_T with the angular ω_t velocity).

Coefficients r_1 and r_2 can be chosen, for example, as follows. If the maximum values are known $\omega_{g1maximum},\omega_{g2maximum},\alpha_{maximum},\beta_{maximum}$, then

$$
r_1=\frac{k_1}{K}=\frac{\omega_{g1maximum}}{\alpha_{maximum}},_1\ r_2=\frac{k_2}{K}=\frac{\omega_{g1maximum}}{\beta_{maximum}}
\tag{20}
$$

taking into account that in orientation mode (equation (18)), $\omega_{g1}=M_x/K$, $\omega_{g1maximum}=$ $=\omega_{t1maximum}$, $\omega_{g2maximum}=\omega_{t2maximum}\cos\lambda_2^*$ and chosen $\omega_{t1maximum}/\alpha_{maximum}=\omega_{t2maximum}/$ $/\beta_{maximum}=r$, results

$$
r_1=r=\frac{\omega_{t1maximum}}{\alpha_{maximum}},r_2=\frac{\omega_{t2maximum}}{\beta_{maximum}}\cos\lambda_2^*=r\cos\lambda_2^*
\tag{21}
$$

with λ_2^* its average value of λ_2.

Rotation of the sighting line (marking) *oz* with the angles α and β, so with angular velocities $\dot{\vec{\alpha}}$ and $\dot{\vec{\beta}}$, will generate gyroscopic torques,

$\vec{M}_{gx} = \vec{K} \times \dot{\vec{\alpha}}$ and $M_{gy_1} = \vec{K}(\cos^2 \lambda_2) \times \times \dot{\vec{\beta}}$ (Fig.2.b and the equations (16)).

Over these gyroscopic torques are superimposed correction torques ($\vec{M}_x^c$ and $\vec{M}_{y1}^c$), (16), $\vec{M}_x^c = \vec{\omega}_{g1} \times \vec{K}, \vec{M}_{y1}^c = \vec{\omega}_{g2} \times \vec{K}(\cos \lambda_2)$. These torques rotate the axis *oz* towards the axis ox_T and this, in turn, rotates with the angular velocity of transport ω_T (having the components ω_{t1} and ω_{t2} along the axes oy_T and oz_T). So, in orientation mode, the two axes (*oz* and ox_T) overlap the equilibrium direction (the line represented by the dashed line); the equilibrium direction marks the overlap of the reference line *oz* (axis TC, that is, the vector $\vec{K}$) over the target line ox_T; $\vec{\omega}_g + \vec{\omega}_t = 0$ ($\omega_{g1} = \omega_{t1}, \omega_{g2} = \omega_{t2} \cos \lambda_2$).

Relative degrees of the dynamic model of GG in relation to the output variables $y_1 = \omega_{g1}$ and $y_2 = \omega_{g2}$ are equal to 2; the equations (18) (in which $\omega_{g1} = \frac{M_x^c}{K} = \frac{k_x}{K} i_x$ and $\omega_{g2} \cos \lambda_2 = \frac{M_{y1}^c}{K} = \frac{k_y}{K} i_y$) can be expressed in the following forms

$$\begin{aligned}
&\ddot{y}_1 = -\frac{f_y - (a_3 + b_1)\omega_{t2}}{b_0} \dot{y}_1 - \frac{\omega_{x_T}\omega_{t1} + \omega_{x_T}^2 \sin \lambda_2^*}{b_0} y_1 - \frac{r_1}{r_2} \frac{\cos^2 \lambda_2^* + (b_1 - a_1)}{b_0} \dot{y}_2 - \\
&- r_1 \frac{a_3 + b_1}{b_0} (\omega_{t1} + \omega_{x_T}\omega_{t2} + \dot{\omega}_{x_T}) y_2 + \frac{a_3 + b_1}{r_2 b_0} + \omega_{x_T}^2 y_1 y_2 + \frac{a_3 + b_1}{r_1 b_0} y_1 \dot{y}_1 - \frac{a_0 + b_0}{r_2 b_0} \cdot \\
&\cdot \omega_{t2} \dot{y}_1 y_2 - \frac{r_1}{r_2^2} \frac{(a_3 + b_1)\omega_{x_T}}{b_0} y_2 \dot{y}_2 - \frac{a_3 + b_1}{r_2} y_1 \dot{y}_2 - \frac{\omega_{x_T}}{r_1 r_2 b_0} y_1 \dot{y}_1 y_2 + \frac{a_0 - r_1 c}{r_2^2 b_0} \cdot \\
&\cdot \dot{y}_1 y_2 \dot{y}_2 - \frac{r_1}{b_0} \frac{k_y}{K} i_y + \frac{N_y^*}{b_0} \\
&\ddot{y}_2 = -\frac{f_x}{a_0} \dot{y}_2 - \frac{\omega_{x_T}}{a_0} y_2 + \frac{1 - d_0 \omega_{x_T}}{a_0} \frac{r_2}{r_1} \dot{y}_1 - \frac{a_0 \dot{\omega}_{x_T} + f_x \omega_{x_T}}{a_0} \frac{r_2}{r_1} y_1 + \frac{c + c_1}{r_1 a_0} (\omega_{t1} + \omega_Y) \cdot \\
&\cdot \dot{y}_1 y_2 - \frac{e_0}{r_1^2 a_0} \dot{y}_1^2 y_2 - \frac{e_0}{r_1 r_2 a_0} \omega_{x_T} \dot{y}_1 y_2 \dot{y}_2 + \frac{r_2}{a_0} \frac{k_x}{K} i_x + \frac{N_x^*}{a_0}
\end{aligned} \tag{22}$$

with N_x^* and N_y^* by forms (19), in which they were replaced λ_1 and λ_2 with their average values λ_1^* and λ_2^*; in (18) the correction moments were expressed

$$M_{y1}^c = k_y i_y, M_x^c = k_x i_x \tag{23}$$

where i_x and i_y are the control currents applied to the two motors in the axes *ox* and oy_1, and k_x and k_y are the coefficients of proportionality with the torque/current dimension.

The system of nonlinear equations (22) (nonlinear dynamics of GG) can be expressed in the form

$$\ddot{\boldsymbol{y}} = \hat{\boldsymbol{v}} + \boldsymbol{\varepsilon}, \hat{\boldsymbol{v}} = \begin{bmatrix} -m_2 y_1 - m_4 y_2 + m_5 y_1 y_2 - m_{12} i_y \\ -n_4 y_1 - n_2 y_2 + n_8 i_x \end{bmatrix} \tag{24}$$

4. CONCLUSIONS

The nonlinear equations of the dynamics of the GG placed on a rocket, relative to an absolute reference trihedron, are derived using the generalized Euler equations, taking into account the angular velocities of the sighting line relative to the trihedron connected to the guidance line, the angular transport velocities of the guide line and the angular velocities of rocket. In the obtained equations, the new variables represented by the angular velocities of the line of sight are introduced ω_{g1} and ω_{g2} ,oriented so that α and β the deviation angles of the sighting line from the guide line (according to Fig.2) cancel out. These angular precession speeds oriented around the cardanic suspension axes are created by gyroscopic effect by the correction moments (16) produced by the control moments (M_x^c and M_{y1}^c) produced by CM1 and CM2 engines.Through the action of these motors, the effects of external disturbances N_x^* and N_y^* are compensated . These effects are due to the angular velocities of the base and orient the line of sight over the guide line. The control moments M_x^c and M_{y1}^c are chosen proportionally to ω_{g1} and ω_{g2} (these are of the form (17), with the proportionality coefficients r_1 and r_2 (respectively, k_1 and k_2) functions of maximum transport angular velocities $\omega_{t1maximum}$ and $\omega_{t2maximum}$ of the guide line and the angles $\alpha_{maximum}$ and $\beta_{maximum}$ of the sighting line relative to the target line (21). The directions of control moments M_x^c and M_{y1}^c are the same as the directions of the gyroscopic torques created by the angular velocities $\vec{\dot{\alpha}}$ and $\vec{\dot{\beta}}$ of the sighting line (Fig.2.b). In orientation mode, according to equations (18) and Fig.2.b, $\omega_{g1} = \omega_{t1}$ and $\omega_{g2} = \omega_{t2}\cos\lambda_2^*$, relations that impose the input vector of GG on the output vector $\boldsymbol{y} = [\omega_{g1}\ \ \omega_{g2}]^T$. For reducing the bearing λ_2 of the sighting line so that $\omega_{g2} \to \omega_{t2}$, the rocket must be ordered through its pilot automatically so that $\lambda_2 \to 0$.

Relative degrees of the nonlinear dynamic model of GG (according to equations (22) in relation to the output vector variables ω_{g1} and ω_{g2} are equal with 2. By dynamic inversion, the vector of control currents i_y and i_x is calculated, these currents are applied to CM2 and CM1 engines.

For the nonlinear dynamic model (22), an adaptive controller is designed to stabilize and orient the line of sight over the guide line, using the concept of dynamic inversion and a neural network.

REFERENCES

[1] B. Fenu, V. Atanasio, *Analysis of gyroscopic–stabilized floating offshore hybrid wind–wave platform*, Journal of Marine Science and Engineering, 8,439, 21 pag., 2020;

[2] B.Xiang, Q. Mu, *Gimbal control stabilized platform for airborne remote sensing systems based on adaptive RBFNN feedback model*, IFAC Journal of Systems and Control, 16, 9 pag., 2021;

[3] Y.Zou, Xu.Lei, *A compound control method of the adaptive neural network and sliding mode control for inertial stable platform,* Neurocomputing, 155, pag.286 – 294, 2015;

[4] S.Liu, Lu, Tianyu, T .Shang, Q.Xia, *Dynamic modeling and coupling characteristic analysis of two–axis rate gyro seeker,* Internațional Journal of Aerospace Engineering, Vol. 1, 14 pag., 2018;

[5] S.Pan, *Robust control of gyro stabilized platform driven by ultrasonic motor*. Sensor and actuators 1, Physical A 261, pag.280 – 287, 2017;

[6] N.C. Townesed, R.A .Shenoi, *Gyrostabilizer vehicular technology,* Transactions of the ASME, Vol. 64, 12 pag, 2011;

[7] J.D.G. Kooijman,J.D.G., A.L. Schwab, J.P. Meijaard. J.P. *Experimental validation of model of an uncontrolled bicycle,* Multibody Systems Dynamics, 19 pag., 2008;

[8] P.F. Wu, L.T. Liu, L. Wang, *A gyro stabilized platform leveling loop for marine gravimeter*, Review of Scientific Instruments, 88, 7 pag, 2017;
[9] S. Dey, S. Halder, M.P. Pandakumar, *Gyroscpic stabilization of two–dimensional gimbals platform using fuzzy logic control,* Internațional Journal of Electrical and Data Communicație, Vol. 2, pag.36 – 42, 2014;
[10] Xu. Zheng, Xi. Zhu, Z. Chen, Yi. Sung, B. Liang, *Dynamic modeling of an unmanned motorcycle and combined balance control with both steriing and double CMGs,* Mechanism and Machine Theory. 169, 23 pag., 2022;
[11] R. Lungu, M. Lungu, C. Efrim, *Attitude adaptive control of sattelites using double–gimbal magnetically suspended control moment gyros*, Aerospace Science and Technology, Vol. 126, 2022;
[12] R. Lungu, *Gyroscopic Equipment and systems, .* University Editory, Craiova, 1997;
R. Lungu, C.A Mihai, *Dynamic and Adaptive Control of Monoaxial GS with GAR. Part 1: Obtaining the Nonliner Model*, IEEE International Conference on Applied and Theoretical Electricity (ICATE), pag.1 – 6, 2024;
[13] R. Lungu, C.A Mihai, *Dynamic and Adaptive Control of Monoaxial GS with GAR. Part 2: Control Arhitecture Design and Validation*, IEEE International Conference on Applied and Theoretical Electricity (ICATE),pag.1 – 6, 2024;
[14] H. T.Li, B. Fang, C. Han, T. Wei, *Study on system disturbance rejection method used in the gimbal servo system of double gimbal magnetically suspended control moment gyro,* Journal of Astronautics, Vol. 30, pag. 2199-2205, 2009;
[15] R. Lungu, M. Lungu, C., Efrim, O. Bombaker, *Backstepping control of double–gimbal control moment gyroscope,* 24 IEEE Internațional Conference on System Teory, Control and Computing, Sinaia, România, pag. 154 – 159, 2020;
[16] R. Lungu, C. Efrim, Z. Zheng, M. Lungu, *Dynamic inversion based of control of DGMSCMGs. Part 2: Control arhitecture design and validation,* IEEE Internațional Conference on Applied and Theoretical Electricty (ICATE), pag.7 – 12, 2021;
[17] R. Lungu, C. Efrim, Z. Zheng, M. Lungu, *Dynamic inversion based of control of DGMSCMGs. Part 1: Obtaining nonlinear model,* IEEE International Conference on Applied and Theoretical Electricty (ICATE), pag.1 – 6, 2021;
[18] D.Su, S. Xu, *The precise control of double gimbal MSCMG based on modal separtion and feedback linearization,* In Proceedings of 2013. International Conference on Electrical Machines and Systems, Korea, pag.1355 – 1360;
[19] H. Li, S. Yang, H. Ren, *Dynamic decoupling control of DGCMG gimbal system via state feedback linearization,* Mechatronics 36, pag. 127-135, 2016;
[20] Ch. Xiaocen, Ch. Maoyin, *Precise control of magnetically double gimbal control moment gyroscope using differențial geometric decoupling method,* In Chinese Journal of Aeronautics, 26(4), pag. 1017 – 1028, 2013;
[21] R. Lungu, M. Lungu, C. Efrim, *Adaptive control of DGMSCMG using dynamic inversion and neural networks,* Advances and Space Research, Vol.68, Nr.8, pag. 3478 – 3494, 2021;
[22] A. Isidori, *Nonlinear control systems,* Springher, Berlin, 1995;
[23] Y. Mousavi, A. Zarei, Z.S. Jahromi, *Robust active fractional– order nonsingular terminal sliding mode stabilizație of three–axis gimbal platform,* ISA Transactions 123, pag.98 – 109, 2022
[24] H. Kojima, R. Nakamura, S. Keshtkar, *Model predictive steering control low for double gimbal scissored–pair control moment gyros,"* Acta Astronautica 183, pag. 273 – 285, 2021.